Available online at www.sciencedirect.com

SciVerse ScienceDirect

Journal of the European Ceramic Society 32 (2012) 1473–1479

www.elsevier.com/locate/jeurceramsoc

Short communication

Welding of yttrium-doped zirconia granules by electric current activated sintering (ECAS): Protrusion formation as a possible intermediate step in the consolidation mechanism

Anne Cordier*, Michel Kleitz, Marlu César Steil

LEPMI, UMR 5279, CNRS, Grenoble INP, Université de Savoie, Université Joseph Fourier, 1130 Rue de la Piscine BP75, 38402 Saint Martin d'Hères, France

Received 9 November 2011; received in revised form 9 December 2011; accepted 13 December 2011
Available online 14 January 2012

Abstract

The basic mechanisms of the current activated/assisted sintering (ECAS) of yttrium-doped zirconia's currently is a controversial issue. To gather more experimental data, we performed two-electrode-experiments (2EE) on staked spherical granules of cubic yttria-stabilised zirconia (YSZ) of diameters ranging from 10 to 100 μm. The observations were focused on the initial welding stage, under currents smaller than 4 A cm^{-2}. The impedance spectroscopy appears to be a sensitive technique to detect the very early welding stage. FEG-SEM analysis reveals protrusion formations at the granule surfaces which are probable intermediate microstructures in the neck formation.

Keywords: A. Sintering; B. Electron microscopy; B. Microstructure; C. Impedance; D. ZrO_2

1. Introduction

The electric current activated/assisted sintering (ECAS) consists in passing an electric current, with a possibly additional applied pressure, throw a green compact or a loose powder at high temperature or during the heating process. The first ECAS patent is attributed to Bloxam in 1906.[1] Amongst the numerous ECAS techniques, Spark Plasma Sintering is the most widely developed. Two electrode experiments (2EE) using AC or DC electrical fields applied during a conventional sintering process have successfully led to dense sintering of Y_2O_3-doped ZrO_2,[2–5] MgO-doped Al_2O_3[6] and Co_2MnO_4.[7] Despite all this research and development work, the consolidation/sintering specific mechanisms are still unclear. It is obviously recognized[3,4,8,9] that the passing of an electrical current through a resistive material induces a Joule heating, but this, on its own, does not fully explain the observed results, except for Grasso et al.[9] It was shown that an electric field retards the grain growth[10,11] but has no significant effect on the grain size distribution.[12] The presence of an electrostatic charge at the grain boundaries and of segregated solute ions, were mentioned as possible explanations along with a decrease in the grain boundary energy and in the solute ion mobility. Cologna and Raj[13] have shown that the electric field should not affect the neck growth rate at the early stage of the sintering during which surface diffusion is the predominant consolidation mechanism. During the early ECAS stage, in a porous body, the current flows through the matrix and the grain boundaries and not along the surfaces where it could affect the surface diffusion. In a review article, Munir et al.[14] pointed out that during the ECAS process, mass transport can be enhanced by electromigration, point defect generation and defect mobility enhancement. Moreover Raj et al.[4] have suggested that, at least, two mechanisms are simultaneously prevalent. In a recent paper[3] devoted to cubic zirconia, it has been strongly recommended to use an AC signal instead of a DC one, in the two-electrode-experiments, to avoid detrimental electrolysis effects. This recommendation applies to all materials becoming ionic conductors at high temperature. The objective of the present study was to perform 2EE using AC signal on pre-sintered YSZ granules to gather new experimental observations, focused on the early stages in the neck formation. Recently, Demirskyi et al.[15] also performed measurements on such a microstructure, but in microwave and SPS equipments.

* Corresponding author. Tel.: +33 4 76 82 65 98; fax: +33 4 76 82 67 77.
E-mail address: annecordier@rocketmail.com (A. Cordier).

0955-2219/$ – see front matter © 2011 Elsevier Ltd. All rights reserved.
doi:10.1016/j.jeurceramsoc.2011.12.022

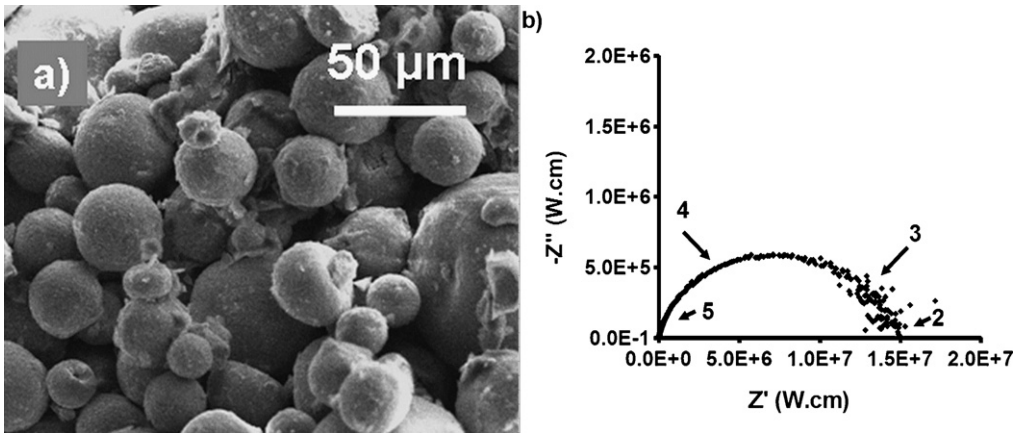

Fig. 1. Characterisation of the softly compacted powder. (a) SEM image of the granules stack. (b) Corresponding impedance diagram measured at 400 °C.

2. Experimental

2.1. Sample processing

Our raw material was the 8 mol.% yttria stabilised zirconia, commercial powder, from Tosoh (TZ-8Y). Its specific surface area is $16 \pm 3\ m^2\ g^{-1}$, it is composed of granules from 15 μm to 140 μm in diameter, formed of 30 nm grains. The powder was calcined at 1300 °C during 24 h to get fairly rigid spheres and also to obtain stable grain sizes; if not, their growth would have interfered with the observed phenomena. This heat treatment does not result in any noticeable inter-granule sintering (in fact, the selection of this calcination temperature results from a compromise between a maximum grain growth and the absence of such an inter-granule sintering). The granules shrunk down to diameters from 10 to 100 μm and the elementary grains grow to 1.2 μm. This calcined powder, called TZ-1300, was then mixed with a binder (PEG 3500) and softly compacted uniaxially under 62 MPa in the form of discs 2.5 mm thick and 10 mm in diameter which were placed in an alumina ring in the sample holder. A typical SEM image of the as-compacted sample is shown in Fig. 1a. It shows that granules are in contact with each other and that their shape integrity is maintained. Each disc was then heated at 800 °C to remove the binder and cooled down to 400 °C for the first impedance spectroscopy measurement. A typical impedance diagram of the as-compacted samples is shown in Fig. 1b. It is an unaltered semicircle, indicating a good electrical homogeneity of the samples.

2.2. 2EE welding equipment and procedures

The experiment disc was placed in the sample holder inside an alumina ring and contacted on each of its faces with a platinum grid 45 mesh, slightly pressed under about 100 g to maintain the contact. A thermocouple was placed close to the sample (<1 cm) to detect variation in the sample temperature. It cannot be pressed in contact with it to avoid any interference with the welding field. All this experimental set-up was introduced inside a furnace operated with its own regulation. The granule welding was performed, under air, with a Pacific Smart Source 115ASX AC power generator, connected to the sample holder and controlled by the UPC Manager V.1.4 software. It allows to applied to the sample, a field adjustable between 0 and 240 V cm^{-1} whilst limiting the resulting electrical current density to a select value up to 10 A cm^{-2} (target current in Table 1). All the electrical parameters were continuously recorded.

In all the welding experiments, the initial reference sample temperature was 902 °C. Initially, an impedance diagram was plotted at this temperature to give an estimate of the sample initial resistivity ($\rho_{bw\text{-}902} = 1700\ \Omega$ cm). The welding field was then increased from 0 V cm^{-1}, by step increments of either 8 V cm^{-1} (slow rate: sr in Table 1), 20 V cm^{-1} (normal rate: nr in Table 1), or 60 V cm^{-1} (fast rate: fr in Table 1) until the current reached the target limit. The duration of all the incremental steps was 1 min except in the 3A-fr experiment where it was 30 s. Examples of the recorded current as a function of time are shown in Fig. 2. As previously observed by Muccillo et al.[3] the first measured current intensities indicate an approximately ohmic behaviour in agreement with the sample initial resistance. On the other hand, as soon as a threshold field was reached (V_{max} in Table 1), typically 180–200 V cm^{-1}, the current increased suddenly (Fig. 2), until the target limit was reached; it was then fixed by the electrical equipment. Then, instantaneously, the equipment voltage

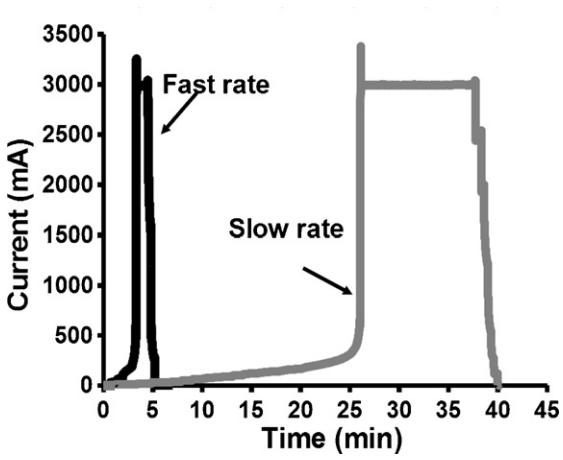

Fig. 2. Typical current versus time variation during 2EE.

Table 1
Experimental conditions of the 2EE.

	Target current		Voltage increment	Stabilisation time	V_{max}	Vwelding	ρ_w	Dwell at Imax	Total duration
	(A)	(A cm^{-2})	(V cm^{-1})	(s)	(V cm^{-1})	(V cm^{-1})	(Ω cm)	(min)	(min)
1A-nr	1	1.3	20	60	200	120	60	10	25
2A-nr	2	2.5	20	60	180	124	45	10	23.5
3A-fr	3	3.8	60	30	200	108	30	2	5
3A-sr	3	3.8	8	60	180	120	27	15	40

decreased to a field value close to 120 V cm^{-1} (V_w in Table 1). This is the indication of the welding occurrence and the resulting decrease in the sample resistance. The sample resistance, and resistivity (ρ_w in Table 1) under the welding conditions can be simply evaluated using the relevant values of the applied field (V_w) and current density (target current).

The thermocouple located close to the sample, gave an indication of any heating of the sample. The maximum recorded temperature was around 930 °C for the 1A-nr, 2A-nr and 3A-fr experiments and 940 °C for 3A-sr. The experiments were arbitrarily stopped when this thermocouple started indicating a temperature decrease. The corresponding times (Dwell time at Imax and total duration) are shown in Table 1.

After completion of the welding process, the sample returned to the rest temperature of 902 °C and a new impedance diagram was plotted to get an estimate of the sample resistivity ($\rho_{aw\text{-}902}$ in Table 2), at this temperature, after the welding. The variations of the sample resistivity from this value to that under the welding conditions (ρ_w in Table 1) allows us to estimate the average sample temperature reached during the welding, referring to the Arrhenius variation law[3]:

$$\rho_T = \rho_0 \exp\left(\frac{-Ea}{kT}\right) \quad (1)$$

For that, we assumed a high temperature activation energy Ea of −0.8 eV.[16] This estimated welding temperature (T_w – Table 2), of the order of 1350–1450 °C, is much higher than that measured by the thermocouple located close to the sample which was of the order of 930 °C.

2.3. Characterisations

For the impedance spectroscopy analysis, a HP impedancemeter (HP 4194A) was used. An AC signal ranging from 100 to 1.5×10^7 Hz in frequency (400 points in this interval) and of 0.3 V amplitude was applied to the sample. The detailed analysis was all done at 400 °C (Fig. 3). Measurements were also performed at 902 °C. Measurements were recorded with a home made software. The Zview software (Scribner Associates Incorporated) was used for fitting the impedance diagram and calculating the relevant parameters. After the welding, the diagrams can be fitted with two semi-circles (Fig. 3d). The corresponding parameters are reported in Table 2.

Microstructure observations of the sample before welding, and after the 1A-nr and 2A-nr experiments were made thanks to a Field Emission Gun SEM (Zeiss Ultra 55) equipped with an energy and angle selective backscattering detector. The samples 3A-sr and 3A-fr were observed with a FEG-ESEM (FEI quanta FEG 250). The estimation of the mean diameter of the grain, in the granules, was made thanks to the ImageJ software (National Institute of Health–USA) with more than 50 measurements.

3. Results and discussion

3.1. Granules welding

The total resistivity of the granule stack before welding, measured at 400 °C ($\rho_{400\text{-}bw}$), is 1.5×10^7 Ω cm. The initial value of the resistivity of all the samples, measured at 902 °C ($\rho_{902\text{-}bw}$), is about 1700 Ω cm. This value is approximative because of interferences with inductive effects and electrode polarizations which cannot be easily separated at this temperature. A huge decrease of the resistivity is measured after the welding experiments ($\rho_{902\text{-}aw}$ – Table 2), the impedance spectroscopy appears as a powerful tool for in situ characterisation of welding experiment.

After a welding current density limited to 1.3 A cm^{-2} (1A-nr), very few microstructure evolutions are observable (Fig. 4a). The surface of the granules is rough, the grain size of the granules is estimated to be the same as before welding (i.e. 1.2 μm). Amongst other details, it can be noted that irregular grains of "dust" are stuck on the granule surfaces. No neck, whatever their size, were formed at the grain contacts (Fig. 4b). However, protrusion formations (see next section and Fig. 5a) may already have established contacts between the granules. The welding temperature evaluated as described above was 1461 °C. The 400 °C impedance diagram shows an enormous variation (Fig. 3a). This light welding has resulted in a sample total resistivity reduction by a factor of about 10, pointing to a strong amelioration of the contacts between the granules. This shows the high sensitivity of the impedance spectroscopy to characterise the electric contacts between YSZ granules.

After a welding current density limited to 2.5 A cm^{-2} (2A-nr), the sample resistance is again strongly reduced by another factor of about 10 (Fig. 3b). The evaluated welding temperature was 1342 °C The microstructure of the granule changes. The surface is less rough and the grain size has grown to about 2.9 μm (Fig. 4c). Necks between granules can be clearly identified (Fig. 4d). They are around 300–500 nm thick.

A limitation of the welding current density to a higher value of 3.8 A cm^{-2} (3A-fr and 3A-sr) does not seem to markedly change the electrical sample characteristics (Fig. 3b and c). The evaluated welding temperature was 1364 °C and 1340 ° C for the

Table 2
Calculated impedance spectroscopy parameters after welding: R is the resistivity, $f°$ is the relaxation frequency and C the specific capacitance of the high (1) and low (2) frequency semicircles.

	$\rho_{902\text{-}aw}$ (Ω cm)	T_w (°C)	ρ_1 (Ω cm)	f°1 (Hz)	C1 (F cm^{-1})	ρ_2 (Ω cm)	$f°2$ (Hz)	C2 (F cm^{-1})
1A-nr	768	1461	3×10^4	7.6×10^5	7×10^{-12}	1.3×10^6	3.6×10^2	3.5×10^{-10}
2A-nr	388	1342	7.2×10^4	6.3×10^5	3.5×10^{-12}	3.3×10^5	4.4×10^3	1.1×10^{-10}
3A-fr	279	1364	1.2×10^5	4.3×10^5	3.1×10^{-12}	2.1×10^5	6.4×10^3	1.1×10^{-10}
3A-sr	231	1340	7.8×10^4	5.7×10^5	3.6×10^{-12}	2.3×10^5	2.4×10^3	2.9×10^{-10}

3A-fr and 3A-sr experiments respectively. A huge grain growth is observed (Fig. 4e), the mean diameter is estimated to be around 4.7 μm, the surface tends to be smoother. Necks can be clearly observed and they seem to be slightly more frequent (Fig. 4f), but their thickness is not obviously different from the 2A-nr sample. Fig. 3c shows that the welding field increase rate does not have a strong influence on the contact electrical characteristics (under the investigated experimental conditions). Changing the dwell time at the limited current (3A-sr) has no obvious consequence on the grain size (mean diameter of 3A-sr sample: 4.9 μm) (Fig. 4g). No difference as well is found for the frequency of the neck formations, neither for their size (Fig. 4h).

As it can be seen in Fig. 3b, the impedance diagrams recorded at 400 °C are all composed of two semi circles. Fig. 3d gives an example of a deconvolution into 2 semicircles. The parameters extracted from such a resolution are given in Table 2. The frequency relaxation of the high frequency semi-circle (f°1 in Table 2) clearly identifies this semi-circle as a response of the intragrains (frequently called "bulk" in the specialized literature). From the corresponding resistivities R1 and specific capacitances C1 one can calculate the average relative dielectric constant of the material (38). Referring to the results published by Steil et al.[17] this indicates a sample porosity of about 45%, in agreement with the value we could evaluate from the microstructure images. The second semi-circle describes the electrical blocking effects at the contacts between the granules but also between the elementary grains. This last contribution decreases with the increase in the grain size. It should therefore be slightly

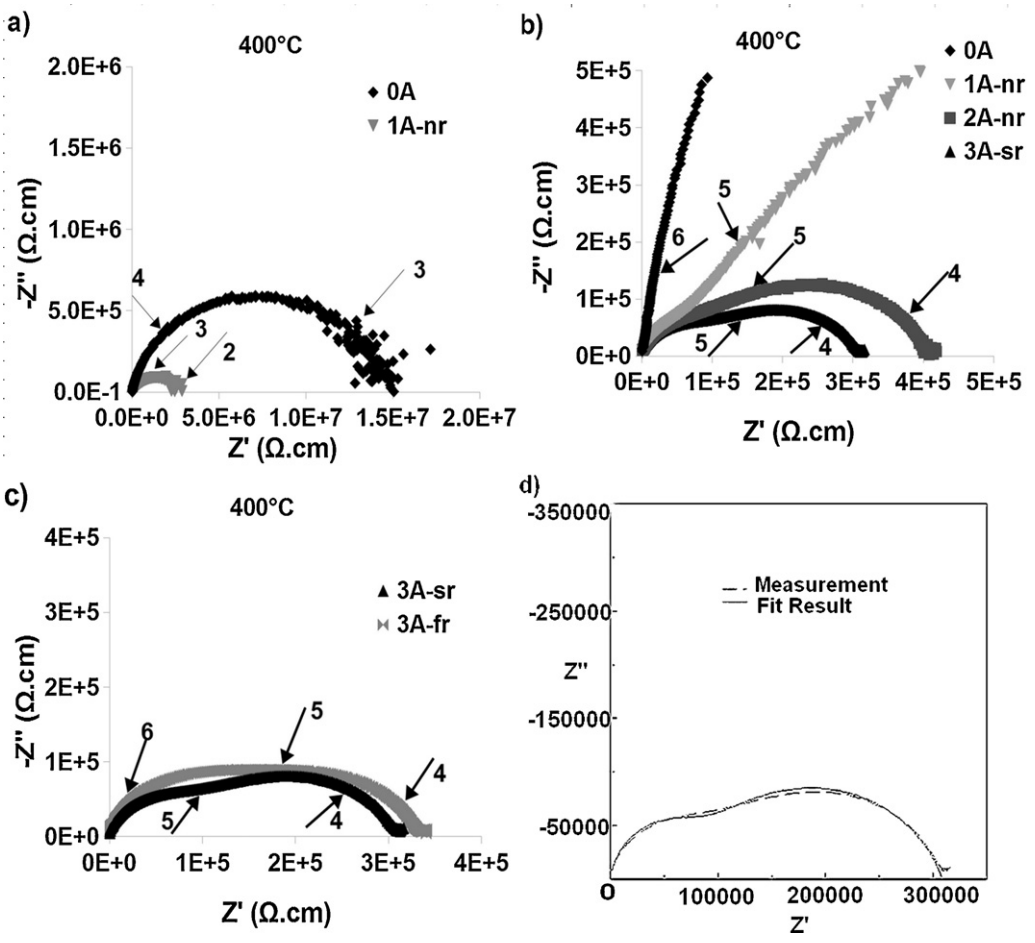

Fig. 3. Impedance spectroscopy diagram of the granule compact measured at 400 °C (the numbers stand for the logarithm of the frequency): (a) general view of the diagrams, (b) zoom in the high frequency area, (c) comparison between the slow rate and the fast rate when limited current is 3A, (d) fitting of the diagram with Zview®.

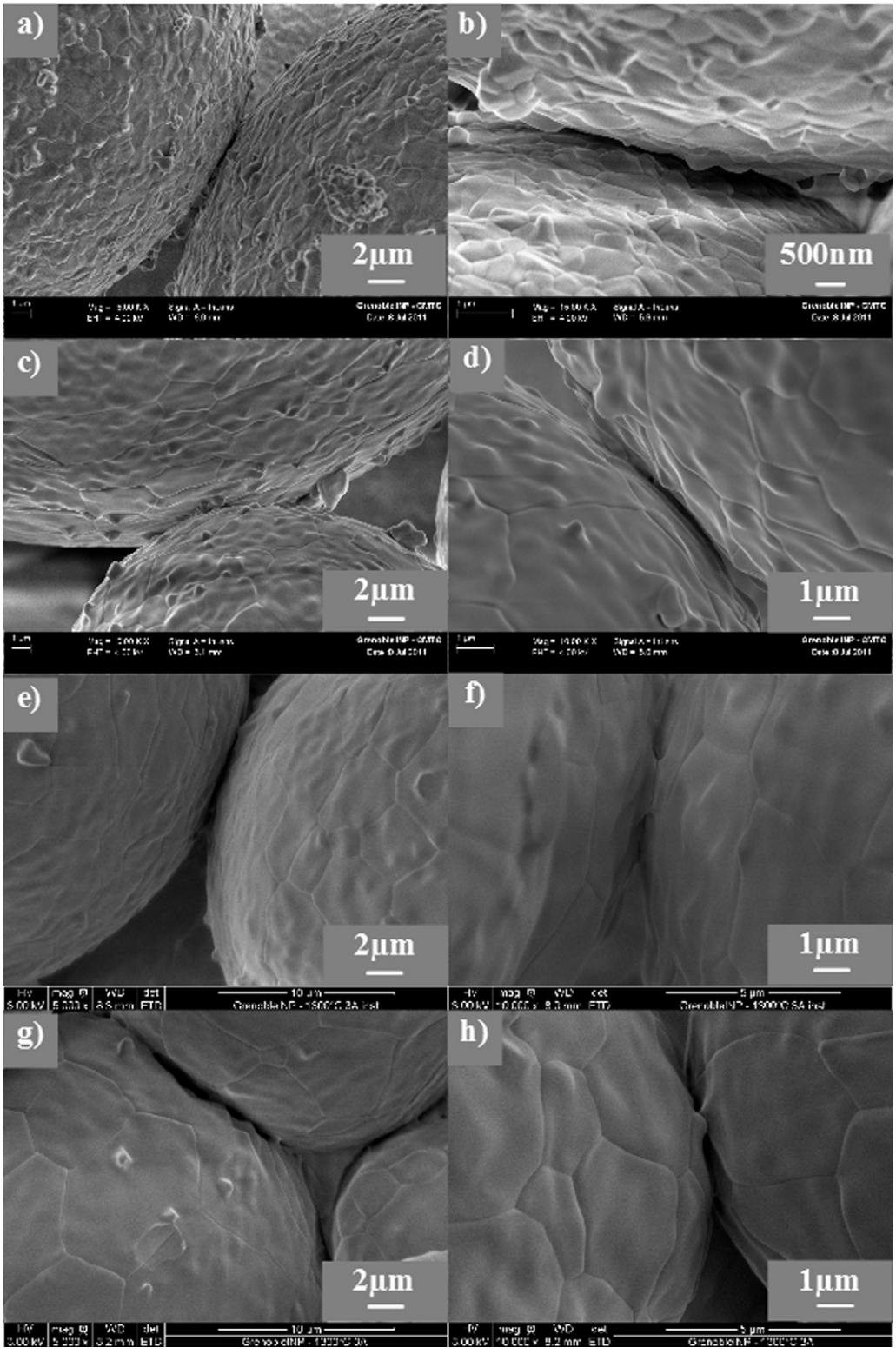

Fig. 4. FEG-SEM observations of the welded stacks. (a and b) 1A-nr; (c and d) 2A-nr; (e and f) 3A-fr; (g and h) 3A-sr.

smaller in the 2A sample and even smaller in the 3A. We can assume that this contribution remain small with respect to that of the granule welding (because of the initial fairly large grain size[17]).

In conclusion, as soon as a current density of 1.3 A cm^{-2} is applied, electrical contacts are improved. However, a current density of 2.5 A cm^{-2} is needed to form neck between pre-sintered granules. Increasing again the current density has only

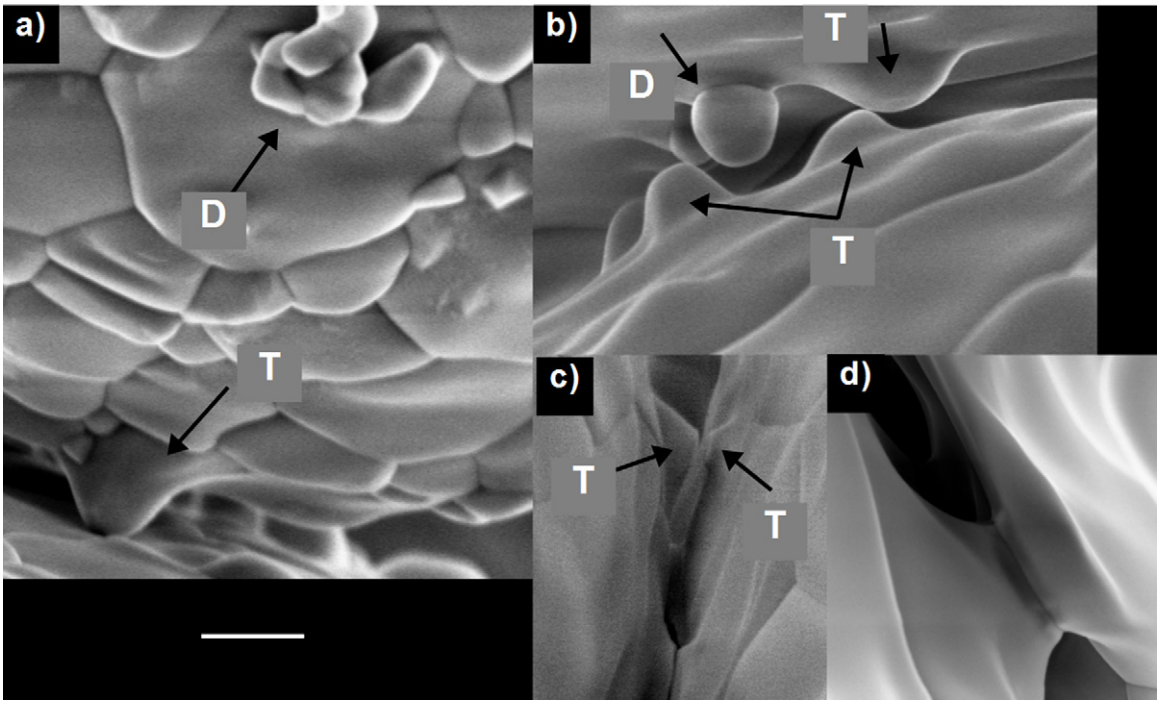

Fig. 5. FEG-SEM observations of the protusions. (a) 1A-nr; (b and d) 2A-nr; (d) 3A-fr. The scale represents 500 nm for (a) and (b), 1.1 μm for (c), 333 nm for (d). "D" means dust and "T" means protusion.

a weak consequence on electrical properties. The microstructure of the granules is greatly affected as soon as a current density of 2.5 A cm^{-2} is applied, in addition with the neck formation, a huge grain growth is observed. Increasing again the current density (3.8 A cm^{-2}), increases the grain growth. As no correlation was found between the welding temperature (T_w) and the grain growth, we can conclude that the grain growth is mostly due to the current density that might affect the grain boundary mobility in these conditions. The two electrodes welding experiments allows to improve contacts between granules without changing the packing of the granule stack.

3.2. Protrusion formation

On the FEG-SEM observations, unexpected microstructure features are detected (Fig. 5). Surprising protrusion formations appear as soon as an AC is applied (Fig. 5a). This feature cannot be mixed up with the dust grains that could be incorporated in the granule surface. Dust grains are more angular (D in Fig. 5a) and are separated from the granule surface by a grain boundary (D in Fig. 5b), whereas the protrusions are smoother and seem to be part of the grain (T in Fig. 5a and b). They appear at the surface of the grain but never at the grain boundary. Moreover, we often observe, on facing surfaces, two protrusion formations, in front of each other (Fig. 5c) that are not yet in contact. Because of the very low probability to incorporate dust grains at the same spot on two different granule surfaces, we can also see this as an indication of a difference in nature between the dust grains and the protrusions. In addition, we can further note that the thickness of the necks (Fig. 5d) is very close to the height of the protrusion formations. The difference in microstructure between incorporated dust and protrusion formations is less obvious after high welding current because of smoother surfaces.

Consequently, we propose that these protrusion formations are the first step in the consolidation mechanism by ECAS and is a consequence of the application of the field. The observation of the protrusions has been made possible because of the thermal treatment of the powder before welding (1300 °C-24 h) that greatly decreases the reactivity of the surface, and also thanks to the high porosity of the stack.

4. Conclusion

In ECAS experiments, the welding of pre-heated TZ-8Y granules, with diameter of about 100 μm, have been performed under various experimental conditions, starting from a rest temperature of 902 °C. Under these experimental conditions, the current might affect the grain boundary mobility. Moreover, a new microstructure feature has been observed. Protrusion formations appear on the surfaces of the granules, in the vicinity of their physical contacts as soon as a current is passed through the material. Using impedance spectroscopy allowed us to detect the early welding stages where contacts between granules could be insured solely by these protrusion formations. After passing currents of the order of 2.5 A cm^{-2}, well formed necks could be seen.

Acknowledgements

This work was partially funded by the French ANR project PIREP2 (n° ANR-2010-VPTT006-04). The authors thank Dr. F.

Roussel Dherbey and Dr. F. Charlot (CMTC, INP Grenoble) for SEM observations.

References

1. Grasso S, Sakka Y, Maizza G. Electric current activated/assisted sintering (ECAS): a review of patents 1906–2008. *Sci Tech Adv Mater* 2009;**10**:053001.
2. Yang D, Conrad H. Enhanced sintering rate of zirconia (3Y-TZP) by application of a small AC electric field. *Scripta Mater* 2010;**63**:328–31.
3. Muccillo R, Kleitz M, Muccillo ENS. Flash grain welding in yttria stabilized zirconia. *J Eur Ceram Soc* 2011;**31**:1517–21.
4. Raj R, Cologna M, Francis JSC. Influence of externally imposed and internally generated electrical fields on grain growth, diffusional creep, sintering and related phenomena in ceramics. *J Am Ceram Soc* 2011;**94**:1941–65.
5. Cologna M, Prette ALG, Raj R. Flash-sintering of cubic yttria-stabilized zirconia at 750 °C for possible use in SOFC manufacturing. *J Am Ceram Soc* 2011;**94**:316–9.
6. Cologna M, Francis JSC, Raj R. Field assisted and flash sintering of alumina and its relationship to conductivity and MgO-doping. *J Eur Ceram Soc* 2011.
7. Prette ALG, Cologna M, Sglavo V, Raj R. Flash-sintering of Co_2MnO_4 spinel for solid oxide fuel cell applications. *J Power Sources* 2011;**196**:2061–5.
8. Munir Za, Anselmi-Tamburini U, Ohyanagi M. The effect of electric field and pressure on the synthesis and consolidation of materials: a review of the spark plasma sintering method. *J Mater Sci* 2006;**41**:763–77.
9. Grasso S, Sakka Y, Rendtorff N, Hu C, Maizza G, Borodianska H, et al. Modeling of the temperature distribution of flash sintered zirconia. *Ceram Soc Jpn* 2011;**119**:144–6.
10. Conrad H, Yang D. Influence of an applied dc electric field on the plastic deformation kinetics of oxide ceramics. *Philos Mag* 2010;**90**: 1141–57.
11. Yang D, Conrad H. Influence of an electric field on the superplastic deformation of 3Y-TZP. *Scripta Mater* 1997;**36**: 1431–5.
12. Starnes S, Conrad H. Grain size distribution in ultrafine-grained yttria-stabilized zirconia deformed without and with an electric field. *Scripta Mater* 2008;**59**:1115–8.
13. Cologna M, Raj R. Surface diffusion-controlled neck growth kinetics in early stage sintering of zirconia, with and without applied DC electrical field. *J Am Ceram Soc* 2011;**94**:391–5.
14. Munir Za, Quach DV, Ohyanagi M. Electric current activation of sintering: a review of the pulsed electric current sintering process. *J Am Ceram Soc* 2011;**94**:1–19.
15. Demirskyi D, Borodianska H, Grasso S, Sakka Y, Vasylkiv O. Microstructure evolution during field-assisted sintering of zirconia spheres. *Scripta Mater* 2011;**65**:683–6.
16. Weller M, Herzog R, Kilo M, Borchardt G, Weber S, Scherrer S. Oxygen mobility in yttria-doped zirconia studied by internal friction, electrical conductivity and tracer diffusion experiments. *Solid State Ionics* 2004;**175**:409–13.
17. Steil MC, Thevenot F, Kleitz M. Densification of yttria-stabilized zirconia. *J Electrochem Soc* 1997;**144**:390.